

ห้องสมุดงานวิจัย สำนักงานคณะกรรมการการวิจัยแห่งชาติ



E47361



VIBRATIONAL SPECTROSCOPIC STUDY AND
THERMAL DECOMPOSITION KINETICS OF
SOME SINGLE AND BINARY METAL
PHOSPHATE HYDRATES

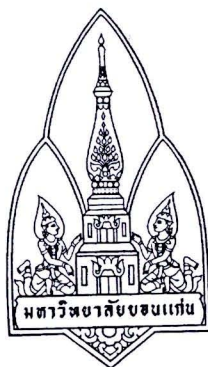
MR. SURASUK BOONTIMA

A THESIS FOR THE DEGREE OF MASTER OF SCIENCE
KHON KAEN UNIVERSITY

2010



E47361



**VIBRATIONAL SPECTROSCOPIC STUDY AND
THERMAL DECOMPOSITION KINETICS OF
SOME SINGLE AND BINARY METAL
PHOSPHATE HYDRATES**



MR. SURASUK BOONTIMA

**A THESIS FOR THE DEGREE OF MASTER OF SCIENCE
KHON KAEN UNIVERSITY**

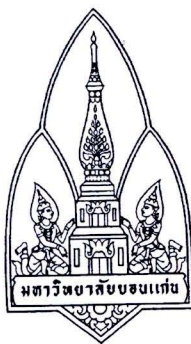
2010

**VIBRATIONAL SPECTROSCOPIC STUDY AND
THERMAL DECOMPOSITION KINETICS OF
SOME SINGLE AND BINARY METAL
PHOSPHATE HYDRATES**

MR. SURASUK BOONTIMA

**A THESIS SUMMITTED IN PARTIAL FULFILMENT OF THE
REQUIREMENTS FOR THE DEGREE OF MASTER OF SCIENCE
IN PHYSICAL CHEMISTRY
GRADUATE SCHOOL
KHON KAEN UNIVERSITY**

2010



THESIS APPROVAL
KHON KAEN UNIVERSITY
FOR
MASTER OF SCIENCE
IN PHYSICAL CHEMISTRY

Thesis Title : Vibrational Spectroscopic Study and Thermal Decomposition Kinetics
of Some Single and Binary Metal Phosphate Hydrates

Author : Mr. Surasuk Boontima

Thesis Examination Committees :

Asst. Prof. Dr. Kunwadee Rangsiwatananon	Chairperson
Asst. Prof. Dr. Chanaiporn Danvirutai	Member
Asst. Prof. Dr. Tipaporn Srithanratana	Member
Asst. Prof. Dr. Jinda Khemprasit	Member
Asst. Prof. Dr. Khatcharin Siriwong	Member

Thesis Advisors :

C. Danvirutai.....Advisor
(Asst. Prof. Dr. Chanaiporn Danvirutai)

Tipaporn Srithanratana.....Co-Advisor
(Asst. Prof. Dr. Tipaporn Srithanratana)

L. Manmart
(Assoc. Prof. Dr. Lampang Manmart)

Dean, Graduate School

K. Sangaroon
(Asst. Prof. Dr. Kiat Sangaroon)

Dean, Faculty of Science

สุรศักดิ์ บุญธิมา. 2553. การศึกษาฟอสเฟตไฮดรตของโลหะเดี่ยวและโลหะคู่ด้วยวิธี

สเปกโทรสโกปีการสั่นและจลนพลศาสตร์การสลายตัวด้วยความร้อน. วิทยานิพนธ์

ปริญญาวิทยาศาสตรมหาบัณฑิต สาขาวิชาเคมีฟิสิกัล บัณฑิตวิทยาลัย

มหาวิทยาลัยขอนแก่น.

อาจารย์ที่ปรึกษาวิทยานิพนธ์: ผศ. ดร. ไฉนพร ด้านวิรุฑัย,

ผศ. ดร. ทิพาภรณ์ ศรีชัยรัตน์

บทคัดย่อ

ได้เตรียมฟอสเฟตไฮดรตโลหะเดี่ยวและโลหะคู่ 7 ชนิดคือ **E47361** $\text{ZnHPO}_4 \cdot \text{H}_2\text{O}$, $\text{Co}(\text{H}_2\text{PO}_4)_2 \cdot 2\text{H}_2\text{O}$, $\text{LiFePO}_4 \cdot 3\text{H}_2\text{O}$, $\text{LiCoPO}_4 \cdot 3\text{H}_2\text{O}$, $\text{LiNiPO}_4 \cdot \text{H}_2\text{O}$, $\text{LiMnPO}_4 \cdot \text{H}_2\text{O}$ และ $\text{Li}_2\text{Zn}(\text{HPO}_4)_2 \cdot \text{H}_2\text{O}$ รวมทั้งสารประกอบคิเวอเรตของไฮดรตเหล่านี้ จำนวนโมลของน้ำในไฮดรตที่เตรียมขึ้นได้ หาโดยอาศัยเทคนิค TG/DTG/DTA และ วิเคราะห์ พีชเซอร์ ส่วนการหาปริมาณโลหะหนัก แมงกานีส โคบอลต์ นิกเกิล และสังกะสี ได้ใช้เทคนิค AAS และการหาปริมาณโลหะลิเทียม ใช้เทคนิค AES โครงสร้างของสารที่เตรียมได้ยืนยันเพิ่มเติมจากผลของ XRD ผลที่ได้จากเทคนิคเหล่านี้ สามารถยืนยันสูตรโมเลกุลของไฮดรตที่เตรียมขึ้นมาได้ว่าเป็นไปตามที่ระบุ พร้อมทั้งได้บันทึกสเปกตรัมการสั่น และวิเคราะห์รายละเอียดของแถบการสั่นโดยอาศัยการวิเคราะห์การแตกออกของสนามสหสัมพันธ์ ผลการศึกษาพบว่า การสั่นแบบโค้งงอของน้ำใน $\text{ZnHPO}_4 \cdot \text{H}_2\text{O}$ และ $\text{Co}(\text{H}_2\text{PO}_4)_2 \cdot 2\text{H}_2\text{O}$ ปรากฏที่ตำแหน่ง 1638 และ 1610 cm^{-1} ตามลำดับ ในสารประกอบ $\text{LiFePO}_4 \cdot 3\text{H}_2\text{O}$ ปรากฏที่ตำแหน่ง 1619 และ 1400 cm^{-1} ในสารประกอบ $\text{LiCoPO}_4 \cdot 3\text{H}_2\text{O}$ ปรากฏที่ตำแหน่ง 1622 และ 1583 cm^{-1} ในสารประกอบ $\text{LiNiPO}_4 \cdot \text{H}_2\text{O}$, $\text{LiMnPO}_4 \cdot \text{H}_2\text{O}$ และ $\text{Li}_2\text{Zn}(\text{HPO}_4)_2 \cdot \text{H}_2\text{O}$ ปรากฏที่ตำแหน่ง 1594 , 1609 และ 1609 cm^{-1} ค่าความถี่การสั่นแบบไม่คู่ควบของหมู่ OH [$\nu_{\text{OH}}(\text{HOD})$] ในสารประกอบฟอสเฟตไฮดรตที่เลือกศึกษานี้ สามารถนำไปประมาณค่าระยะห่างระหว่างออกซิเจนของน้ำกับออกซิเจนของแอนไอออน ($\text{R}_{\text{O} \dots \text{O}}$) และเอนทัลปีของพันธะไฮโดรเจน [ΔH_{H} (kJ/mol)] ของ $\text{LiFePO}_4 \cdot 3\text{H}_2\text{O}$, $\text{LiCoPO}_4 \cdot 3\text{H}_2\text{O}$, $\text{LiNiPO}_4 \cdot \text{H}_2\text{O}$ และ $\text{LiMnPO}_4 \cdot \text{H}_2\text{O}$ ได้ โดยใช้สมการ $\text{R}_{\text{O} \dots \text{O}} = 3.764 (\text{\AA}) - 0.169 (\text{\AA}) \ln \Delta \nu_{\text{OH}}(\text{HOD})/\text{cm}^{-1} \text{\AA}$ และ $-\Delta H_{\text{H}} = 1.286 + 0.0418 \Delta \nu_{\text{OH}}(\text{HOD})/\text{cm}^{-1} \text{kJ/mol}$ ตามลำดับ พบว่าค่าระยะ $\text{R}_{\text{O} \dots \text{O}}$ และ $-\Delta H_{\text{H}}$ มีค่าเท่ากับ 2.787 , 2.781 , 2.765 , 2.755\AA , และ 14.9 , 15.3 , 16.7 , 17.4 kJ/mol OH ตามลำดับ การสลายตัวทางความร้อนของไฮดรตที่เตรียมได้ศึกษาโดยเทคนิค DSC และพลังงานกระตุ้นหาได้โดยวิธีของ Ozawa และ Kissinger

E47361

การสลายตัวทางความร้อนของ $\text{ZnHPO}_4 \cdot \text{H}_2\text{O}$ พบว่ามีสองขั้นตอน ขั้นตอนแรกเป็นการหลุดออกของน้ำผลึกส่วนขั้นตอนที่สองเป็นการปลดปล่อยน้ำที่เป็นองค์ประกอบในแอนไอออน HPO_4^{2-} แล้วเปลี่ยนไปเป็น $\text{P}_2\text{O}_7^{4-}$ พลังงานกระตุ้นของขั้นตอนแรกและขั้นตอนที่สองที่คำนวณโดยวิธีของ Ozawa ได้เท่ากับ 258.7 และ 252.6 kJ/mol ตามลำดับ และเท่ากับ 250.0 และ 242.2 kJ/mol ตามลำดับ โดยวิธี Kissinger การสลายตัวทางความร้อนของ $\text{Co}(\text{H}_2\text{PO}_4)_2 \cdot 2\text{H}_2\text{O}$ สังเกตเห็นสองขั้นตอน ขั้นตอนแรกเป็นการหลุดออกของน้ำผลึกส่วนขั้นตอนที่สองเป็นการปลดปล่อยน้ำที่เป็นองค์ประกอบในแอนไอออน H_2PO_4^- แล้วเปลี่ยนไปเป็น $\text{P}_4\text{O}_{12}^{4-}$ พลังงานกระตุ้นของขั้นตอนแรกและขั้นตอนที่สองที่คำนวณโดยวิธีของ Ozawa ได้เท่ากับ 112.9 และ 217.3 kJ/mol ตามลำดับ และเท่ากับ 104.5 และ 207.7 kJ/mol ตามลำดับ โดยวิธี Kissinger การสลายตัวทางความร้อนของ $\text{LiFePO}_4 \cdot 3\text{H}_2\text{O}$ มีสามขั้นตอน พลังงานกระตุ้นของขั้นตอนที่หนึ่ง สอง และสาม ที่คำนวณโดยวิธีของ Ozawa เท่ากับ 98.0, 121.9 และ 253.3 kJ/mol ตามลำดับ และเท่ากับ 91.4, 114.1 และ 243.8 kJ/mol ตามลำดับ โดยวิธี Kissinger การสลายตัวทางความร้อนของ $\text{LiCoPO}_4 \cdot 3\text{H}_2\text{O}$ มีสามขั้นตอน พลังงานกระตุ้นของขั้นตอนที่หนึ่ง สอง และสาม ที่คำนวณโดยวิธีของ Ozawa เท่ากับ 117.0, 459.3 และ 556.9 kJ/mol ตามลำดับ และเท่ากับ 109.4, 450.8 และ 548.8 kJ/mol โดยวิธี Kissinger การสลายตัวทางความร้อนของ $\text{LiNiPO}_4 \cdot \text{H}_2\text{O}$ มีหนึ่งขั้นตอน มีพลังงานกระตุ้นเท่ากับ 142.5 และ 134.1 kJ/mol โดยวิธีของ Ozawa และ Kissinger ตามลำดับ การสลายตัวทางความร้อนของ $\text{LiMnPO}_4 \cdot \text{H}_2\text{O}$ เกิดขึ้นหนึ่งขั้นตอน มีพลังงานกระตุ้นเท่ากับ 115.5 และ 107.5 kJ/mol โดยวิธีของ Ozawa และ Kissinger ตามลำดับ พบว่าในสารประกอบ $\text{LiFePO}_4 \cdot 3\text{H}_2\text{O}$, $\text{LiCoPO}_4 \cdot 3\text{H}_2\text{O}$, $\text{LiNiPO}_4 \cdot \text{H}_2\text{O}$ และ $\text{LiMnPO}_4 \cdot \text{H}_2\text{O}$ การสูญหายของมวลในแต่ละขั้นตอนสอดคล้องกับจำนวนโมลของน้ำผลึกที่หลุดออกจากโครงผลึกและผลิตภัณฑ์สุดท้ายของการสลายตัวของไฮเดรตเหล่านี้จะได้สารปราศจากน้ำที่สอดคล้องกันคือ LiFePO_4 , LiCoPO_4 , LiNiPO_4 และ LiMnPO_4 ตามลำดับ ซึ่งนำไปใช้ในอุตสาหกรรมลิเทียมแบตเตอรี่ต่อไปได้ ส่วนการสลายตัวทางความร้อนของ $\text{Li}_2\text{Zn}(\text{HPO}_4)_2 \cdot \text{H}_2\text{O}$ มีสองขั้นตอนโดยขั้นตอนแรกเป็นการหลุดออกของน้ำผลึกมีพลังงานกระตุ้นเท่ากับ 102.6 และ 213.5 kJ/mol และขั้นตอนที่สองเป็นการปลดปล่อยน้ำที่เป็นองค์ประกอบในแอนไอออน HPO_4^{2-} แล้วเปลี่ยนไปเป็น $\text{P}_2\text{O}_7^{4-}$ มีพลังงานกระตุ้นเท่ากับ 94.8 และ 204.0 kJ/mol โดยวิธีของ Ozawa และ Kissinger ตามลำดับ จากการศึกษากระบวนการกำจัดน้ำออกจากโครงสร้างและการนำน้ำกลับเข้ามาในโครงสร้างอีกนั้นเป็นกระบวนการผันกลับ ภายใต้อุณหภูมิที่ไม่เกิน 200 °C

Surasuk Boontima. 2010. **Vibrational Spectroscopic Study and Thermal Decomposition Kinetics of some Single and Binary Metal Phosphate Hydrates.** Master of Science Thesis in Physical Chemistry, Graduate School, Khon Kaen University.

Thesis Advisors : Asst. Prof. Dr. Chanaiporn Danvirutai,
Asst. Prof. Dr. Tipaporn Srithanratana

ABSTRACT

E 47361

Seven single and binary metal phosphate hydrates, namely $\text{ZnHPO}_4 \cdot \text{H}_2\text{O}$, $\text{Co}(\text{H}_2\text{PO}_4)_2 \cdot 2\text{H}_2\text{O}$, $\text{LiFePO}_4 \cdot 3\text{H}_2\text{O}$, $\text{LiCoPO}_4 \cdot 3\text{H}_2\text{O}$, $\text{LiNiPO}_4 \cdot \text{H}_2\text{O}$, $\text{LiMnPO}_4 \cdot \text{H}_2\text{O}$ and $\text{Li}_2\text{Zn}(\text{HPO}_4)_2 \cdot \text{H}_2\text{O}$, and their partially deuterated analogue were synthesized. The mole number of water of all hydrates were determined by TG/DTG/DTA and Karl Fischer methods. The metal contents of these hydrates were determined by using the AAS for Fe, Mn, Co, Ni and Zn, while Li was determined by AES methods. Their structures were additionally characterized by XRD method. The results confirm the hydrate formula. Their vibrational spectra were recorded on an FTIR/FT Raman spectrophotometer and analyzed by using the correlation field splitting analysis. The water bending vibrational bands of $\text{ZnHPO}_4 \cdot \text{H}_2\text{O}$ and $\text{Co}(\text{H}_2\text{PO}_4)_2 \cdot 2\text{H}_2\text{O}$ were observed at 1638 and 1610 cm^{-1} , respectively. The water bending vibrational bands of $\text{LiFePO}_4 \cdot 3\text{H}_2\text{O}$ were observed at 1619 and 1400 cm^{-1} , while those of $\text{LiCoPO}_4 \cdot 3\text{H}_2\text{O}$ were found at 1622 and 1583 cm^{-1} . The single water bending vibration of $\text{LiNiPO}_4 \cdot \text{H}_2\text{O}$, $\text{LiMnPO}_4 \cdot \text{H}_2\text{O}$ and $\text{Li}_2\text{Zn}(\text{HPO}_4)_2 \cdot \text{H}_2\text{O}$ were observed at 1594, 1609 and 1609 cm^{-1} , respectively. The observed uncoupled ν_{OH} (HOD) vibrations in selected phosphate hydrates lead to the estimation of the internuclear distances between water oxygen and anion oxygen ($R_{\text{O} \cdots \text{O}}$) and enthalpies of hydrogen bonding ($-\Delta H_{\text{H}}$) of $\text{LiFePO}_4 \cdot 3\text{H}_2\text{O}$, $\text{LiCoPO}_4 \cdot 3\text{H}_2\text{O}$, $\text{LiNiPO}_4 \cdot \text{H}_2\text{O}$ and $\text{LiMnPO}_4 \cdot \text{H}_2\text{O}$ by using equation $R_{\text{O} \cdots \text{O}} = 3.764 (\text{\AA}) - 0.169 (\text{\AA}) \ln \Delta \nu_{\text{OH}}(\text{HOD})/\text{cm}^{-1} \text{\AA}$ and $-\Delta H_{\text{H}} = 1.286 + 0.0418 \Delta \nu_{\text{OH}}(\text{HOD})/\text{cm}^{-1} \text{ kJ/mol}$, respectively. The $R_{\text{O} \cdots \text{O}}$ and $-\Delta H_{\text{H}}$ were found to be 2.787, 2.781, 2.765, 2.755 \AA and 14.9, 15.3, 16.7 and 17.4 kJ/mol OH, respectively. Thermal decomposition of synthesized hydrates were studied by using DSC method

E47361

and the activation energy values were calculated by Ozawa and Kissinger methods. The thermal decomposition of $\text{ZnHPO}_4 \cdot \text{H}_2\text{O}$ was observed to be in two steps. The first step corresponds to the removal of water of crystallization molecule from the structure. The second step can be described as an additional dehydration from the HPO_4^{2-} anions and transformed into $\text{P}_2\text{O}_7^{4-}$ ions. The activation energy values of the first and second steps calculated by Ozawa method were found to be 258.7 and 252.6 kJ/mol, and 250.0 and 242.2 kJ/mol for Kissinger method, respectively. The thermal decomposition of $\text{Co}(\text{H}_2\text{PO}_4)_2 \cdot 2\text{H}_2\text{O}$ was observed to be in two steps. The first step corresponds to the removal of water of crystallization molecule from the structure. The second step can be described as an additional dehydration from the HPO_4^{2-} anions and transforms into $\text{P}_4\text{O}_{12}^{4-}$ ions. The activation energy values of the first and second steps calculated by Ozawa method were found to be 112.9 and 217.3 kJ/mol, respectively, and 104.5 and 207.7 kJ/mol for Kissinger method. The thermal decomposition of $\text{LiFePO}_4 \cdot 3\text{H}_2\text{O}$ appeared in three steps. The activation energy values of the first, second and third steps calculated by Ozawa method were found to be 98.0, 121.9 and 253.3 kJ/mol, and 91.4, 114.1 and 243.8 kJ/mol for Kissinger method, respectively. The thermal decomposition of $\text{LiCoPO}_4 \cdot 3\text{H}_2\text{O}$ was observed to be in three steps. The activation energy values of the first, second and third steps calculated by Ozawa method were found to be 117.1, 459.3 and 556.9 kJ/mol, and 109.4, 450.8 and 548.8 kJ/mol for Kissinger method, respectively. The thermal decomposition of $\text{LiNiPO}_4 \cdot \text{H}_2\text{O}$ was observed to be in one step and the activation energy values were found to be 142.5 and 134.1 kJ/mol for the Ozawa and Kissinger methods, respectively. The thermal decomposition of $\text{LiMnPO}_4 \cdot \text{H}_2\text{O}$ exhibited one step and the activation energy values were found to be 115.5 and 107.5 kJ/mol for the Ozawa and Kissinger methods, respectively. The observed mass losses of the $\text{LiFePO}_4 \cdot 3\text{H}_2\text{O}$, $\text{LiCoPO}_4 \cdot 3\text{H}_2\text{O}$, $\text{LiNiPO}_4 \cdot \text{H}_2\text{O}$ and $\text{LiMnPO}_4 \cdot \text{H}_2\text{O}$ correspond to the mole number of water of crystallization. The anhydrous forms are LiFePO_4 , LiCoPO_4 , LiNiPO_4 and LiMnPO_4 , those can be further used in the lithium ion battery industry. The thermal decomposition of $\text{Li}_2\text{Zn}(\text{HPO}_4)_2 \cdot \text{H}_2\text{O}$ exhibited two steps of mass losses. The first one corresponds to the removal of water of crystallization molecule from the structure. The second one can be described as an additional dehydration from the HPO_4^{2-} anions and transforms into $\text{P}_2\text{O}_7^{4-}$ ions. The study of the dehydration and

E47361

rehydration processes in $\text{Li}_2\text{Zn}(\text{HPO}_4)_2 \cdot \text{H}_2\text{O}$ illustrated that the water molecules can be removed and rehydrated under the condition of lower than 200 °C.

**The goodness of the present thesis is dedicated to my beloved parents and the
entire teaching staff.**

ACKNOWLEDGEMENTS

I would like to express my sincere gratitude to my advisor, Asst. Prof. Dr. Chanaiporn Danvirutai, for her excellent supervision, inspiring guidance and encouragement throughout this research. I am grateful to my co – advisor, Asst. Prof. Dr. Tipaporn Srithanratana for her invaluable advice and helpful criticism.

I would like to thank Assoc. Prof. Dr. Nithima Khaorapapong for her kind guidance about the measurement of thermal properties of hydrates by using TG/DTG/DTA technique. I also would like to acknowledge Mr. Nath Phuwongpah for the suggestion in preparation and operation of the AAS and AES.

I gratefully acknowledge the department of chemistry, faculty of science, Khon Kaen University for providing the facilities throughout. I also wish to thank the Center of Excellence for Innovation in Chemistry (PERCH-CIC) for the financial support.

The appreciation is also expressed to my friends, Miss Pittayagorn Noisong, Mr. Boonprasert Wondee for their kindness, readiness to help and being great friends.

Finally, I am grateful to my parents for their support, understanding and encouragement throughout my study.

Surasuk Boontima

TABLE OF CONTENTS

	Page
ABSTRACT (IN THAI)	i
ABSTRACT (IN ENGLISH)	iii
DEDICATION	vi
ACKNOWLEDGEMENT	vii
TABLE OF CONTENTS	viii
LIST OF TABLES	xii
LIST OF FIGURES	xvii
LIST OF ABBREVIATIONS	xxvii
CHAPTER I INTRODUCTION	1
1.1 Background and Rationales of Study	1
1.2 Objective of the Research	4
1.3 Scope of the Study	4
1.4 Research Expectation	5
CHAPTER II LITERATURE REVIEW	7
2.1 Structure of Solid Hydrates	7
2.2 Hydrogen Bonding Interaction	8
2.3 Angle Dependence of Hydrogen Bond	10
2.4 Distance Dependence of O – H...Y Hydrogen Bond	12
2.5 The Relationship between $\nu_{OH}(HOD)$ or $\nu_{OD}(HOD)$ and $R_{O...O}$	13
2.6 Correlation between $\nu_{OH}(HOD)$ and ΔH_H and Badger-Bauer Rule	14
2.7 Vibrational Spectroscopic Studies of Crystalline Hydrates	15
2.8 Phosphate Ion (PO_4^{3-})	19
2.9 Experimental Techniques	22
2.10 Thermal Analysis Techniques	30
2.11 Isotope Dilution Technique	37

TABLE OF CONTENTS (Cont.)

	Page
2.12 Thermal Decomposition Kinetic Analysis	38
2.13 Symmetry in Structural Chemistry	41
2.14 Information about Selected Hydrates	42
CHAPTER III EXPERIMENTAL	49
3.1 General Experimental	49
3.2 Instruments and Chemicals	50
3.3 Preparation of the Selected Hydrates	51
3.4 Determination of Water of Crystallization	53
3.5 Determination of Metal Content in Hydrates by AAS Technique	55
3.6 Vibrational Spectroscopic Method	58
3.7 The Study on the Thermal Decomposition Kinetics of Selected Hydrates	60
3.8 The Study on the Reversible Hydration of $\text{Li}_2\text{Zn}(\text{HPO}_4)_2 \cdot \text{H}_2\text{O}$	60
CHAPTER IV RESULTS AND DISCUSSION	63
4.1 Physical Properties of the Synthesized Hydrates	63
4.2 Determination of Water of Crystallization of Synthesized Hydrates	63
4.3 Determination of Metal Content in the Synthesized Hydrates	70
4.4 Thermal Decomposition of Some Selected Hydrated	73
4.5 X-Ray Powder Diffraction (XRD) Results	78
4.6 Vibrational Spectroscopic Study of Synthesized Hydrates	83
4.7 Vibrational Spectra of Deuterated Metal Phosphate Hydrates	103
4.8 FT Raman Spectra of Some Selected Hydrates	118
4.9 Correlation Field Splitting Analysis	123
4.10 Calculation of $\text{R}_{\text{O} \dots \text{O}}$ Distance and Enthalpy of Hydrogen Bonding ($-\Delta H_{\text{H}}$)	130
4.11 The Study on the Thermal Decomposition Kinetics	132

TABLE OF CONTENTS (Cont.)

	Page
4.12 Reversible Hydration of Selected Hydrates	162
CHAPTER V CONCLUSION	165
5.1 Zinc Hydrogen Phosphate Monohydrate ($\text{ZnHPO}_4 \cdot \text{H}_2\text{O}$)	165
5.2 Cobalt Dihydrogen Phosphate Dihydrate ($\text{Co}(\text{H}_2\text{PO}_4)_2 \cdot 2\text{H}_2\text{O}$)	166
5.3 Lithium Ferrous Phosphate Trihydrates ($\text{LiFePO}_4 \cdot 3\text{H}_2\text{O}$)	167
5.4 Lithium Cobalt Phosphate Trihydrates ($\text{LiCoPO}_4 \cdot 3\text{H}_2\text{O}$)	168
5.5 Lithium Nickel Phosphate Monohydrate ($\text{LiNiPO}_4 \cdot \text{H}_2\text{O}$)	169
5.6 Lithium Manganese Phosphate Monohydrate ($\text{LiMnPO}_4 \cdot \text{H}_2\text{O}$)	170
5.7 Dilithium Zinc Hydrogen Phosphate Monohydrate ($\text{Li}_2\text{Zn}(\text{HPO}_4)_2 \cdot \text{H}_2\text{O}$)	171
REFERENCES	173
APPENDICES	179
APPENDIX A - Calculation of Water of Crystallization from Karl Fischer Method	183
- Calculation of Water of Crystallization from Differential Thermal Gravimetry	
- Calculation of Metal Content in Synthesized Hydrates from Atomic Absorption Spectroscopy (AAS) and Atomic Emission Spectroscopy (AES)	
APPENDIX B - Mulliken Symbols	217
- Character Tables	
- Correlation Tables	
- Space Group and Site Symmetries	
- Primitive and Centered lattices	
APPENDIX C - Vibrational and Librational Modes of a Water Molecule	225
- Normal Modes of Vibration of Tetrahedral $\text{XY}_4\text{-T}_d$ Molecule	

TABLE OF CONTENTS (Cont.)

	Page
APPENDIX D FTIR Spectrum of KBr	231
APPENDIX E Instruments	235
APPENDIX F Publications	241
VITAE	257

LIST OF TABLES

	Page
Table 2.1 Classification of water molecules in solid hydrates with respect to their lone pair coordination	7
Table 2.2 Vibrational band position ranges (cm^{-1}) of the water in hydrates	17
Table 2.3 Vibrational band position (cm^{-1}) of the H_2O , D_2O and HDO molecules	18
Table 2.4 The vibrational frequencies of PO_4^{3-} , HPO_4^{2-} , H_2PO_4^- and H_3PO_4 (cm^{-1})	21
Table 2.5 The differences of principles of TG, DTG, DTA and DSC techniques	36
Table 2.6 $T_d - C_s - D_{2h}^{16}$ correlation table of phosphate ions (PO_4^{3-}) in $\text{LiFePO}_4 \cdot 3\text{H}_2\text{O}$, $\text{LiCoPO}_4 \cdot 3\text{H}_2\text{O}$, $\text{LiNiPO}_4 \cdot \text{H}_2\text{O}$ and $\text{LiMnPO}_4 \cdot \text{H}_2\text{O}$	45
Table 2.7 The $C_{2v} - C_1 - C_{2v}^7$ correlation table for the three internal water modes and the water librational modes	46
Table 2.8 The $C_{2v} - C_s - C_{2v}^7$ correlation table for the three internal water modes and the water librational modes (zy plane preserved)	47
Table 2.9 The $C_{2v} - C_s - C_{2v}^7$ correlation table for the three internal water modes and the water librational modes (xz plane preserved)	48
Water molecule internal vibrations (xz plane preserved)	
Table 3.1 FTIR band positions of polystyrene reference film (cm^{-1})	59
Table 4.1 Physical properties of synthesized hydrates	63
Table 4.2 The percentage of weight loss, transition temperature, and calculated mole number of crystallization water per mole of anhydrous salt (n) in synthesized hydrates	68
Table 4.3 The percentage of water and blank solution ($\text{CH}_3\text{OH} : \text{HNO}_3$) and sample the mole number of water of crystallization per mole of anhydrous salt (n) determined by Karl Fischer method	69

LIST OF TABLES (Cont.)

	Page
Table 4.4 The metal contents in prepared hydrates form AAS and AES techniques	72
Table 4.5 Vibrational band positions (cm^{-1}) and the possible assignment in three replications of $\text{ZnHPO}_4 \cdot \text{H}_2\text{O}$ using KBr pellet technique	96
Table 4.6 Vibrational band positions (cm^{-1}) and the possible assignment in three replications of $\text{Co}(\text{H}_2\text{PO}_4)_2 \cdot \text{H}_2\text{O}$ using KBr pellet technique	97
Table 4.7 Vibrational band positions (cm^{-1}) and the possible assignment in three replications of $\text{LiFePO}_4 \cdot 3\text{H}_2\text{O}$ using KBr pellet technique	98
Table 4.8 Vibrational band positions (cm^{-1}) and the possible assignment in three replications of $\text{LiCoPO}_4 \cdot 3\text{H}_2\text{O}$ using KBr pellet technique	99
Table 4.9 Vibrational band positions (cm^{-1}) and the possible assignment in three replications of $\text{LiNiPO}_4 \cdot \text{H}_2\text{O}$ using KBr pellet technique	100
Table 4.10 Vibrational band positions (cm^{-1}) and the possible assignment in three replications of $\text{LiMnPO}_4 \cdot \text{H}_2\text{O}$ using KBr pellet technique	101
Table 4.11 Vibrational band positions (cm^{-1}) and the possible assignment in three replications of $\text{Li}_2\text{Zn}(\text{HPO}_4)_2 \cdot \text{H}_2\text{O}$ using KBr pellet technique	102
Table 4.12 FTIR band positions (cm^{-1}) and the possible assignment in three replications of $\text{LiFePO}_4 \cdot 3\text{H}_2\text{O}$ -dx using KBr pellet technique	113
Table 4.13 FTIR band positions (cm^{-1}) and the possible assignment in three replications of $\text{LiCoPO}_4 \cdot 3\text{H}_2\text{O}$ -dx using KBr pellet technique	114
Table 4.14 FTIR band positions (cm^{-1}) and the possible assignment in three replications of $\text{LiNiPO}_4 \cdot \text{H}_2\text{O}$ -dx using KBr pellet technique	115

LIST OF TABLES (Cont.)

	Page
Table 4.15 FTIR band positions (cm^{-1}) and the possible assignment in three replications of $\text{LiMnPO}_4 \cdot \text{H}_2\text{O} \cdot \text{dx}$ using KBr pellet technique	116
Table 4.16 FTIR band positions (cm^{-1}) and the possible assignment in three replications of $\text{Li}_2\text{Zn}(\text{HPO}_4)_2 \cdot \text{H}_2\text{O} \cdot \text{dx}$ using KBr pellet technique	117
Table 4.17 FTIR and FT Raman vibration frequencies (cm^{-1}) of $\text{LiMnPO}_4 \cdot \text{H}_2\text{O}$ and its deuterated analogue ($\text{LiMnPO}_4 \cdot \text{H}_2\text{O} \cdot \text{dx}$)	121
Table 4.18 FTIR and FT Raman vibration frequencies (cm^{-1}) of $\text{Li}_2\text{Zn}(\text{HPO}_4)_2 \cdot \text{H}_2\text{O}$ and its deuterated analogue ($\text{Li}_2\text{Zn}(\text{HPO}_4)_2 \cdot \text{H}_2\text{O} \cdot \text{dx}$).	122
Table 4.19 $T_d - C_s - C_{2h}$ correlation field splitting of phosphate ions (PO_4^{3-}) in $\text{ZnHPO}_4 \cdot \text{H}_2\text{O}$ and $\text{Co}(\text{H}_2\text{PO}_4)_2 \cdot 2\text{H}_2\text{O}$.	124
Table 4.20 $C_{2v} - C_s - D_{2h}$ correlation field splitting of H_2O in $\text{ZnHPO}_4 \cdot \text{H}_2\text{O}$ and $\text{Co}(\text{H}_2\text{PO}_4)_2 \cdot 2\text{H}_2\text{O}$	124
Table 4.21 $T_d - C_s - D_{2h}^{16}$ correlation field splitting of phosphate ions (PO_4^{3-}) in $\text{LiFePO}_4 \cdot 3\text{H}_2\text{O}$, $\text{LiCoPO}_4 \cdot 3\text{H}_2\text{O}$, $\text{LiNiPO}_4 \cdot \text{H}_2\text{O}$ and $\text{LiMnPO}_4 \cdot \text{H}_2\text{O}$ (xy plane preserved)	126
Table 4.22 $T_d - C_s - D_{2h}^{16}$ correlation field splitting of phosphate ions (PO_4^{3-}) in $\text{LiFePO}_4 \cdot 3\text{H}_2\text{O}$, $\text{LiCoPO}_4 \cdot 3\text{H}_2\text{O}$, $\text{LiNiPO}_4 \cdot \text{H}_2\text{O}$ and $\text{LiMnPO}_4 \cdot \text{H}_2\text{O}$ (zx plane preserved)	127
Table 4.23 $T_d - C_s - D_{2h}^{16}$ correlation field splitting of phosphate ions (PO_4^{3-}) in $\text{LiFePO}_4 \cdot 3\text{H}_2\text{O}$, $\text{LiCoPO}_4 \cdot 3\text{H}_2\text{O}$, $\text{LiNiPO}_4 \cdot \text{H}_2\text{O}$ and $\text{LiMnPO}_4 \cdot \text{H}_2\text{O}$ (yz plane preserved)	128
Table 4.24 $C_{2v} - C_s - D_{2h}^{16}$ correlation field splitting of H_2O in $\text{LiFePO}_4 \cdot 3\text{H}_2\text{O}$, $\text{LiCoPO}_4 \cdot 3\text{H}_2\text{O}$, $\text{LiNiPO}_4 \cdot \text{H}_2\text{O}$ and $\text{LiMnPO}_4 \cdot \text{H}_2\text{O}$ (zx plane preserved)	129
Table 4.25 $C_{2v} - C_s - D_{2h}^{16}$ correlation field splitting of H_2O in $\text{LiFePO}_4 \cdot 3\text{H}_2\text{O}$, $\text{LiCoPO}_4 \cdot 3\text{H}_2\text{O}$, $\text{LiNiPO}_4 \cdot \text{H}_2\text{O}$ and $\text{LiMnPO}_4 \cdot \text{H}_2\text{O}$ (yz plane preserved)	129

LIST OF TABLES (Cont.)

	Page
Table 4.26 The Observed $\nu_{\text{OH}}(\text{HOD})$, $\Delta\nu_{\text{OH}}(\text{HOD})$, estimated of $R_{\text{O} \dots \text{O}}$ distance and enthalpy of hydrogen bonding ($-\Delta H_{\text{H}}$) of the synthesized hydrate	131
Table 4.27 DSC data for Ozawa and Kissinger plots of $\text{ZnHPO}_4 \cdot \text{H}_2\text{O}$	133
Table 4.28 Activation energies E_a and correlation coefficient (r^2) calculated by Ozawa and Kissinger method for the dehydration of $\text{ZnHPO}_4 \cdot \text{H}_2\text{O}$	136
Table 4.29 DSC data for Ozawa and Kissinger plots of $\text{Co}(\text{H}_2\text{PO}_4)_2 \cdot 2\text{H}_2\text{O}$	137
Table 4.30 Activation energies E_a and correlation coefficient (r^2) calculated by Ozawa and Kissinger method for the dehydration of $\text{Co}(\text{H}_2\text{PO}_4)_2 \cdot 2\text{H}_2\text{O}$	140
Table 4.31 DSC data for Ozawa and Kissinger plots of $\text{LiFePO}_4 \cdot 3\text{H}_2\text{O}$	141
Table 4.32 Activation energies E_a and correlation coefficient (r^2) calculated by Ozawa and Kissinger method for the dehydration of $\text{LiFePO}_4 \cdot 3\text{H}_2\text{O}$	145
Table 4.33 DSC experimental data for Ozawa and Kissinger plots of $\text{LiCoPO}_4 \cdot 3\text{H}_2\text{O}$	146
Table 4.34 Activation energies E_a and correlation coefficient (r^2) calculated by Ozawa and Kissinger methods for the dehydration of $\text{LiCoPO}_4 \cdot 3\text{H}_2\text{O}$	150
Table 4.35 DSC data for Ozawa and Kissinger plot of $\text{LiNiPO}_4 \cdot \text{H}_2\text{O}$	151
Table 4.36 Activation energies E_a and correlation coefficient (r^2) calculated by Ozawa and Kissinger methods for the dehydration of $\text{LiNiPO}_4 \cdot \text{H}_2\text{O}$	153
Table 4.37 DSC data for Ozawa and Kissinger plot of $\text{LiMnPO}_4 \cdot \text{H}_2\text{O}$	154

LIST OF TABLES (Cont.)

	Page
Table 4.38 Activation energies E_a and correlation coefficient (r^2) calculated by Ozawa and Kissinger methods for the dehydration of $\text{LiMnPO}_4 \cdot \text{H}_2\text{O}$	156
Table 4.39 DSC data for Ozawa and Kissinger plot of $\text{Li}_2\text{Zn}(\text{HPO}_4)_2 \cdot \text{H}_2\text{O}$	158
Table 4.40 Activation energies E_a and correlation coefficient (r^2) calculated by Ozawa and Kissinger methods for the dehydration of $\text{Li}_2\text{Zn}(\text{HPO}_4)_2 \cdot \text{H}_2\text{O}$	160
Table 4.41 The pre-exponential factor (A) of synthesized hydrates calculated by Ozawa and Kissinger methods	162
Table A.1 Summary of Mulliken symbols used for various species of vibrations	219
Table A.2 Symmetry elements, symmetry operations, character tables and correlation tables for point and space groups	220
Table A.3 Vibrational frequencies of H_2O , HOD and D_2O (cm^{-1}) in vapor state	227
Table A.4 Observed water bands (cm^{-1}) in hydrates	228
Table A.5 Vibrational frequencies (cm^{-1}) of PO_4^{3-}	229

LIST OF FIGURES

	Page
Figure 1.1	1
A schematic illustration of relative proportions of phosphate ions in solution at different pH levels in a Ca – H ₃ PO ₄ system. The dashed line shows the upper limit on available P in solution imposed by the solubility of calcium phosphates above pH 6.5 or of iron and aluminum phosphates below pH 6.5. ^[1]	
Figure 1.2	3
The subunit of MHPO ₄ .H ₂ O (a) and structure of the ring layers of MHPO ₄ .H ₂ O (M = Zn, Co, Ni) viewing down the c-axis direction.(b)	
Figure 2.1	7
Coordination of water molecules in solid hydrates	
Figure 2.2	8
Various structures of hydrogen bonds	
Figure 2.3	9
The geometry of an isolated water molecule	
Figure 2.4	10
Potential energy curves of water dimer with different orientations calculated by quantum chemical method, A: repulsion potential B: linear dimer (Clementi), C: cyclic dimer (Clementi)	
Figure 2.5	11
(a) H-bond interaction between a donor system X-H and the lone pair of electron of an acceptor Y depends on the bond angle β between X-H axes of lone-pair of electron orbital. X-H bond is “donor bond” and H...Y is acceptor bond and (b) “Bifurcated H-bond” on H of X-H group with two proton acceptor Y ₁ , and Y ₂ , R _{X...Y1} and R _{X...Y2} are the distances from atom X to Y ₁ and Y ₂ , and the H-bond angle are β_1 and β_2 , respectively.	
Figure 2.6	14
Correlation of uncoupled ν_{OH} band position (cm ⁻¹) with O...O distances	
Figure 2.7	16
Vibrational modes (internal modes) and librational modes of a water molecule	
Figure 2.8	20
Normal modes of vibration of PO ₄ ³⁻ (T _d) ion	
Figure 2.9	24
Block diagram of atomic absorption spectrophotometer (AAS)	
Figure 2.10	25
Block diagram of atomic emission spectrophotometer (AES)	

LIST OF FIGURES (Cont.)

	Page
Figure 2.11 Karl-Fischer method for determination of water. The conventional burette titration with visual detection of the end point to imprecise results. Thus, a cell containing two small platinum electrodes is used. As long as no iodine is present in the solution, the current between the electrodes is weak. When excess iodine is present in the solution the equivalence point is reached, a significant current is registered	27
Figure 2.12 Diagram of principle infrared absorption	29
Figure 2.13 Principle of Raman spectroscopy (a) Elastic, or Rayleigh scattering (b) Inelastic, or Raman scattering (c) Anti-Stokes and Stokes transition	30
Figure 2.14 Schematic single – stage TG curve	31
Figure 2.15 Schematic diagram of classical DTA apparatus	33
Figure 2.16 Schematic illustration of the measured sample temperature as a function of time for a polymer subjected to a linear heating ramp, and the corresponding DTA curve. In the region of the phase transitions the programmed and measured sample temperatures deviate significantly	34
Figure 2.17 Type of DSC	37
Figure 2.18 Coordination of HOD molecule in the D ₂ O surrounding (a) and H ₂ O surrounding (b)	38
Figure 3.1 FTIR spectra of standard polystyrene film	58
Figure 3.2 FTIR spectrum of KBr powder in the region 4000-370 cm ⁻¹	60
Figure 4.1 TG/DTG curves of LiFePO ₄ ·3H ₂ O at the heating rate 10 °C min ⁻¹ in N ₂ atmosphere	64
Figure 4.2 TG/DTG curves of LiCoPO ₄ ·3H ₂ O at the heating rate 10 °C min ⁻¹ in N ₂ atmosphere	65

LIST OF FIGURES (Cont.)

	Page
Figure 4.3 TG/DTG curves of $\text{LiNiPO}_4 \cdot \text{H}_2\text{O}$ at the heating rate $10^\circ\text{C min}^{-1}$ in N_2 atmosphere.	65
Figure 4.4 TG/DTG curves of $\text{LiMnPO}_4 \cdot 3\text{H}_2\text{O}$ at the heating rate $10^\circ\text{C min}^{-1}$ in N_2 atmosphere	66
Figure 4.5 TGA/DTG curves of $\text{Li}_2\text{Zn}(\text{HPO}_4)_2 \cdot \text{H}_2\text{O}$ at the heating rate $10^\circ\text{C min}^{-1}$ in N_2 atmosphere	66
Figure 4.6 DSC curve of $\text{ZnHPO}_4 \cdot \text{H}_2\text{O}$ at the heating rate $10^\circ\text{C min}^{-1}$	73
Figure 4.7 DSC curve of $\text{Co}(\text{H}_2\text{PO}_4)_2 \cdot 2\text{H}_2\text{O}$ at the heating rate $10^\circ\text{C min}^{-1}$	74
Figure 4.8 DSC curve of $\text{LiFePO}_4 \cdot 3\text{H}_2\text{O}$ at the heating rate $10^\circ\text{C min}^{-1}$	74
Figure 4.9 DSC curve of $\text{LiCoPO}_4 \cdot 3\text{H}_2\text{O}$ at the heating rate $10^\circ\text{C min}^{-1}$	75
Figure 4.10 DSC curve of $\text{LiNiPO}_4 \cdot \text{H}_2\text{O}$ at the heating rate $10^\circ\text{C min}^{-1}$	75
Figure 4.11 DSC curve of $\text{LiMnPO}_4 \cdot \text{H}_2\text{O}$ at the heating rate $10^\circ\text{C min}^{-1}$	76
Figure 4.12 DSC curve of $\text{Li}_2\text{Zn}(\text{HPO}_4)_2 \cdot \text{H}_2\text{O}$ at the heating rate $10^\circ\text{C min}^{-1}$	76
Figure 4.13 The XRD patterns of $\text{ZnHPO}_4 \cdot \text{H}_2\text{O}$ (a) and calcined product at 450°C (b)	80
Figure 4.14 The XRD patterns of $\text{Co}(\text{H}_2\text{PO}_4)_2 \cdot 2\text{H}_2\text{O}$ (a) and calcined product at 450°C (b)	80
Figure 4.15 The XRD patterns of $\text{LiFePO}_4 \cdot 3\text{H}_2\text{O}$ (a) and calcined product at 450°C (b)	81
Figure 4.16 The XRD patterns of $\text{LiCoPO}_4 \cdot 3\text{H}_2\text{O}$ (a) and calcined product at 450°C (b)	81
Figure 4.17 The XRD patterns of $\text{LiNiPO}_4 \cdot \text{H}_2\text{O}$ (a) and calcined product at 450°C (b)	82
Figure 4.18 The XRD patterns of $\text{LiMnPO}_4 \cdot \text{H}_2\text{O}$ (a) and calcined product at 450°C (b)	82

LIST OF FIGURES (Cont.)

	Page
Figure 4.19 The XRD patterns of $\text{Li}_2\text{Zn}(\text{HPO}_4)_2 \cdot \text{H}_2\text{O}$ (a), calcined product at 200 °C (b) and calcined product at 450 °C (c)	83
Figure 4.20 FTIR spectra of $\text{ZnHPO}_4 \cdot \text{H}_2\text{O}$ (three replications) in the region of 4000-370 cm^{-1} (KBr)	84
Figure 4.21 FTIR spectra of $\text{Co}(\text{H}_2\text{PO}_4)_2 \cdot \text{H}_2\text{O}$ (three replications) in the region of 4000-370 cm^{-1} (KBr)	84
Figure 4.22 FTIR spectra of $\text{LiFePO}_4 \cdot 3\text{H}_2\text{O}$ (three replications) in the region of 4000-370 cm^{-1} (KBr)	85
Figure 4.23 FTIR spectra of $\text{LiCoPO}_4 \cdot 3\text{H}_2\text{O}$ (three replications) in the region of 4000-370 cm^{-1} (KBr)	85
Figure 4.24 FTIR spectra of $\text{LiNiPO}_4 \cdot \text{H}_2\text{O}$ (three replications) in the region of 4000-370 cm^{-1} (KBr)	86
Figure 4.25 FTIR spectra of $\text{LiMnPO}_4 \cdot \text{H}_2\text{O}$ (three replications) in the region of 4000-370 cm^{-1} (KBr)	86
Figure 4.26 FTIR spectra of $\text{Li}_2\text{Zn}(\text{HPO}_4)_2 \cdot \text{H}_2\text{O}$ (three replications) in the region of 4000-370 cm^{-1} (KBr)	87
Figure 4.27 FTIR band positions in the OH stretching and bending region of ZnHPO_4 (three replications, KBr)	87
Figure 4.28 FTIR band positions in the OH stretching and bending region of $\text{Co}(\text{H}_2\text{PO}_4)_2 \cdot 2\text{H}_2\text{O}$ (three replications, KBr)	88
Figure 4.29 FTIR band positions in the OH stretching and bending region of $\text{LiFePO}_4 \cdot 3\text{H}_2\text{O}$ (three replications, KBr)	88
Figure 4.30 FTIR band positions in the OH stretching and bending region of $\text{LiCoPO}_4 \cdot 3\text{H}_2\text{O}$ (three replications, KBr)	89
Figure 4.31 FTIR band positions in the OH stretching and bending region of $\text{LiNiPO}_4 \cdot \text{H}_2\text{O}$ (three replications, KBr)	89
Figure 4.32 FTIR band positions in the OH stretching and bending region of $\text{LiMnPO}_4 \cdot \text{H}_2\text{O}$ (three replications, KBr)	90

LIST OF FIGURES (Cont.)

	Page
Figure 4.33 FTIR band positions in the OH stretching and bending region of $\text{Li}_2\text{Zn}(\text{HPO}_4)_2 \cdot \text{H}_2\text{O}$ (three replications, KBr)	90
Figure 4.34 FTIR band positions in the region of PO_4^{3-} vibrational of $\text{ZnHPO}_4 \cdot \text{H}_2\text{O}$ (three replications, KBr)	92
Figure 4.35 FTIR band positions in the region of PO_4^{3-} vibrational of $\text{Co}(\text{H}_2\text{PO}_4)_2 \cdot 2\text{H}_2\text{O}$ (three replications, KBr)	93
Figure 4.36 FTIR band positions in the region of PO_4^{3-} vibrational of $\text{LiFePO}_4 \cdot 3\text{H}_2\text{O}$ (three replications, KBr)	93
Figure 4.37 FTIR band positions in the region of PO_4^{3-} vibrational of $\text{LiCoPO}_4 \cdot 3\text{H}_2\text{O}$ (three replications, KBr)	94
Figure 4.38 FTIR band positions in the region of PO_4^{3-} vibrational of $\text{LiNiPO}_4 \cdot \text{H}_2\text{O}$ (three replications, KBr)	94
Figure 4.39 FTIR band positions in the region of PO_4^{3-} vibrational of $\text{LiMnPO}_4 \cdot \text{H}_2\text{O}$ (three replications, KBr)	95
Figure 4.40 FTIR band positions in the region of PO_4^{3-} vibrational of $\text{Li}_2\text{Zn}(\text{HPO}_4)_2 \cdot \text{H}_2\text{O}$ (three replications, KBr)	95
Figure 4.41 FTIR spectra of $\text{LiFePO}_4 \cdot 3\text{H}_2\text{O}$ -dx (three replications) in the region of $4000\text{-}370\text{ cm}^{-1}$ (KBr)	103
Figure 4.42 FTIR spectra of $\text{LiFePO}_4 \cdot 3\text{H}_2\text{O}$ -dx (three replications) in the range of $4000\text{-}2400$; $1900\text{-}1300\text{ cm}^{-1}$ (a) and $1300\text{-}370\text{ cm}^{-1}$ (b) regions (KBr)	104
Figure 4.43 FTIR spectra of $\text{LiCoPO}_4 \cdot 3\text{H}_2\text{O}$ -dx (three replications) in the region of $4000\text{-}370\text{ cm}^{-1}$ (KBr)	105
Figure 4.44 FTIR spectra of $\text{LiCoPO}_4 \cdot 3\text{H}_2\text{O}$ -dx (three replications) in the range of $4000\text{-}1250$ (a) and $1200\text{-}370\text{ cm}^{-1}$ (b) regions (KBr)	106
Figure 4.45 FTIR spectra of $\text{LiNiPO}_4 \cdot \text{H}_2\text{O}$ -dx (three replications) in the region of $4000\text{-}370\text{ cm}^{-1}$ (KBr)	107

LIST OF FIGURES (Cont.)

	Page
Figure 4.46 FTIR spectra of $\text{LiNiPO}_4 \cdot \text{H}_2\text{O} \cdot \text{dx}$ (three replications) in the range of $4000\text{-}1250\text{ cm}^{-1}$ and $1250\text{-}370\text{ cm}^{-1}$ regions (KBr)	108
Figure 4.47 FTIR spectra of $\text{LiMnPO}_4 \cdot \text{H}_2\text{O} \cdot \text{dx}$ (three replications) in the region of $4000\text{-}370\text{ cm}^{-1}$ (KBr)	109
Figure 4.48 FTIR spectra of $\text{LiMnPO}_4 \cdot \text{H}_2\text{O} \cdot \text{dx}$ (three replications) in the range of $4000\text{-}2300$; $1750\text{-}1200\text{ cm}^{-1}$ (a) and $1400\text{-}370\text{ cm}^{-1}$ regions (KBr)	110
Figure 4.49 FTIR spectra of $\text{Li}_2\text{Zn}(\text{HPO}_4)_2 \cdot \text{H}_2\text{O} \cdot \text{dx}$ (three replications) in the region of $4000\text{-}370\text{ cm}^{-1}$ (KBr)	111
Figure 4.50 FTIR spectra of $\text{Li}_2\text{Zn}(\text{HPO}_4)_2 \cdot \text{H}_2\text{O} \cdot \text{dx}$ (three replications) in the range of $4000\text{-}1300\text{ cm}^{-1}$ (a) and $1200\text{-}370\text{ cm}^{-1}$ regions (KBr)	112
Figure 4.51 FT Raman spectrum of $\text{LiMnPO}_4 \cdot \text{H}_2\text{O}$ recorded on a Perkin Elmer Spectrum GX spectrophotometer in the region of $4000 - 250\text{ cm}^{-1}$ (64 scans)	118
Figure 4.52 FT Raman spectrum of $\text{LiMnPO}_4 \cdot \text{H}_2\text{O} \cdot \text{dx}$ recorded on a Perkin Elmer Spectrum GX spectrophotometer in the region of $4000 - 250\text{ cm}^{-1}$ (64 scans)	119
Figure 4.53 FT Raman spectrum of $\text{Li}_2\text{Zn}(\text{HPO}_4)_2 \cdot \text{H}_2\text{O}$ recorded on a Perkin Elmer Spectrum GX spectrophotometer in the region of $4000 - 250\text{ cm}^{-1}$ (64 scans)	119
Figure 4.54 FT Raman spectrum of $\text{Li}_2\text{Zn}(\text{HPO}_4)_2 \cdot \text{H}_2\text{O} \cdot \text{dx}$ recorded on a Perkin Elmer Spectrum GX spectrophotometer in the region of $4000 - 250\text{ cm}^{-1}$ (64 scans)	120
Figure 4.55 DSC curves of the synthesized $\text{ZnHPO}_4 \cdot \text{H}_2\text{O}$ at different heating rates: a = 5, b = 10, c = 20, d = 30 and e = $40\text{ }^\circ\text{C min}^{-1}$ in N_2 atmosphere	133
Figure 4.56 Ozawa plot for the first step of dehydration of $\text{ZnHPO}_4 \cdot \text{H}_2\text{O}$	134

LIST OF FIGURES (Cont.)

	Page
Figure 4.57 Ozawa plot for the second step of decomposition of $\text{ZnHPO}_4 \cdot \text{H}_2\text{O}$	134
Figure 4.58 Kissinger plot for the first step of dehydration of $\text{ZnHPO}_4 \cdot \text{H}_2\text{O}$	135
Figure 4.59 Kissinger plot for the second step of decomposition of $\text{ZnHPO}_4 \cdot \text{H}_2\text{O}$	135
Figure 4.60 DSC curves of the synthesized $\text{Co}(\text{H}_2\text{PO}_4)_2 \cdot 2\text{H}_2\text{O}$ at different heating rates: a = 5, b = 10, c = 20, d = 30 and e = 40 °C min ⁻¹ in N ₂ atmosphere	137
Figure 4.61 Ozawa plot for the first step of dehydration of $\text{Co}(\text{H}_2\text{PO}_4)_2 \cdot 2\text{H}_2\text{O}$	138
Figure 4.62 Ozawa plot for the second step of decomposition of $\text{Co}(\text{H}_2\text{PO}_4)_2 \cdot 2\text{H}_2\text{O}$	138
Figure 4.63 Kissinger plot for the first step of dehydration of $\text{Co}(\text{H}_2\text{PO}_4)_2 \cdot 2\text{H}_2\text{O}$	139
Figure 4.64 Kissinger plot for the second step of decomposition of $\text{Co}(\text{H}_2\text{PO}_4)_2 \cdot 2\text{H}_2\text{O}$	139
Figure 4.65 DSC curves of the synthesized $\text{LiFePO}_4 \cdot 3\text{H}_2\text{O}$ at different heating rates: a = 5, b = 10, c = 20, d = 30 and e = 40 °C min ⁻¹ in N ₂ atmosphere	141
Figure 4.66 Ozawa plot for the first step of dehydration of $\text{LiFePO}_4 \cdot 3\text{H}_2\text{O}$	142
Figure 4.67 Ozawa plot for the second step of dehydration of $\text{LiFePO}_4 \cdot 3\text{H}_2\text{O}$	142
Figure 4.68 Ozawa plot for the third step of dehydration of $\text{LiFePO}_4 \cdot 3\text{H}_2\text{O}$	143
Figure 4.69 Kissinger plot for the first step of dehydration of $\text{LiFePO}_4 \cdot 3\text{H}_2\text{O}$	143
Figure 4.70 Kissinger plot for the second step of dehydration of $\text{LiFePO}_4 \cdot 3\text{H}_2\text{O}$	144

LIST OF FIGURES (Cont.)

	Page
Figure 4.71 Kissinger for the third step of dehydration of $\text{LiFePO}_4 \cdot 3\text{H}_2\text{O}$	144
Figure 4.72 DSC curves of the synthesized $\text{LiCoPO}_4 \cdot 3\text{H}_2\text{O}$ at different heating rates: a = 5, b = 10, c = 20, d = 30 and e = 40 °C min ⁻¹ in N ₂ atmosphere	146
Figure 4.73 Ozawa plot for the first step of dehydration of $\text{LiCoPO}_4 \cdot 3\text{H}_2\text{O}$	147
Figure 4.74 Ozawa plot the second step of dehydration of $\text{LiCoPO}_4 \cdot 3\text{H}_2\text{O}$	147
Figure 4.75 Ozawa plot for the third step of dehydration of $\text{LiCoPO}_4 \cdot 3\text{H}_2\text{O}$	148
Figure 4.76 Kissinger plot for the first step of dehydration of $\text{LiCoPO}_4 \cdot 3\text{H}_2\text{O}$	148
Figure 4.77 Kissinger plot for the second step of dehydration of $\text{LiCoPO}_4 \cdot 3\text{H}_2\text{O}$	149
Figure 4.78 Kissinger plot for the third step of dehydration of $\text{LiCoPO}_4 \cdot 3\text{H}_2\text{O}$	149
Figure 4.79 DSC curves of the synthesized $\text{LiNiPO}_4 \cdot \text{H}_2\text{O}$ at different heating rates: a = 5, b = 10, c = 20, d = 30 and e = 40 °C min ⁻¹ in N ₂ atmosphere	151
Figure 4.80 Ozawa plot of dehydration of $\text{LiNiPO}_4 \cdot \text{H}_2\text{O}$	152
Figure 4.81 Kissinger plot of dehydration of $\text{LiNiPO}_4 \cdot \text{H}_2\text{O}$	152
Figure 4.82 DSC curves of the synthesized $\text{LiMnPO}_4 \cdot \text{H}_2\text{O}$ at different heating rates: a = 5, b = 10, c = 20, d = 30 and e = 40 °C min ⁻¹ in N ₂ atmosphere	154
Figure 4.83 Ozawa plot of dehydration of $\text{LiMnPO}_4 \cdot \text{H}_2\text{O}$	155
Figure 4.84 Kissinger plot of dehydration of $\text{LiMnPO}_4 \cdot \text{H}_2\text{O}$	156
Figure 4.85 DSC curves of the synthesized $\text{Li}_2\text{Zn}(\text{HPO}_4)_2 \cdot \text{H}_2\text{O}$ at different heating rates: a = 5, b = 10, c = 20, d = 30 and e = 40 °C min ⁻¹ in N ₂ atmosphere	157
Figure 4.86 Ozawa plot the first step of dehydration of $\text{Li}_2\text{Zn}(\text{HPO}_4)_2 \cdot \text{H}_2\text{O}$	158
Figure 4.87 Ozawa plot for the second step of decomposition of $\text{Li}_2\text{Zn}(\text{HPO}_4)_2 \cdot \text{H}_2\text{O}$	159

LIST OF FIGURES (Cont.)

	Page
Figure 4.88 Kissinger plot for the first step of dehydration of $\text{Li}_2\text{Zn}(\text{HPO}_4)_2 \cdot \text{H}_2\text{O}$	159
Figure 4.89 Kissinger plot for the second step $\text{Li}_2\text{Zn}(\text{HPO}_4)_2 \cdot \text{H}_2\text{O}$	160
Figure 4.90 The DSC curves of: (a) the synthesized sample, (b) dehydration of sample and (c) the rehydration of sample	163
Figure 4.91 The FTIR spectra of: (a) the calcined product at 200 °C and (b) the dehydrated sample exposed to moisture at room temperature for 2 h	164
Figure A.1 Calibration curve for the determination of iron by AAS	212
Figure A.2 Calibration curve for the determination of cobalt by AAS	212
Figure A.3 Calibration curve for the determination of nickel by AAS	213
Figure A.4 Calibration curve for the determination of manganese by AAS	213
Figure A.5 Calibration curve for the determination of zinc by AAS	214
Figure A.6 Calibration curve for the determination of lithium in $\text{LiCoPO}_4 \cdot 3\text{H}_2\text{O}$ and $\text{LiNiPO}_4 \cdot \text{H}_2\text{O}$ by AES	214
Figure A.7 Calibration curve for determination of lithium of $\text{LiFePO}_4 \cdot 3\text{H}_2\text{O}$, $\text{LiMnPO}_4 \cdot \text{H}_2\text{O}$ and $\text{Li}_2\text{Zn}(\text{HPO}_4)_2 \cdot \text{H}_2\text{O}$	215
Figure A.8 Vibrational and librational modes of a water molecule	227
Figure A.9 Vibrational modes of PO_4^{3-} with T_d point group	228
Figure A.10 Normal modes of vibration for an XY_4 (T_d) symmetry	229
Figure A.11 FTIR spectrum of KBr pellet in the region of 4000-370 cm^{-1} recorded on a Perkin Elmer FTIR spectrum GX spectrophotometer	233
Figure A.12 FTIR/ FT Raman Spectrophotometer, Perkin Elmer Spectrum GX	237
Figure A.13 Karl Fischer Automatic Titrator (Metrohm 798 MPT Titrino)	237
Figure A.14 Differential Scanning Calorimeter (DSC), Perkin Elmer Pyris One	238

LIST OF FIGURES (Cont.)

	Page
Figure A.15 Thermal Gravimetric Analyzer, Differential Thermal Gravimetric, and Differential Thermal Analyzer (TGA/DTG/DTA), Perkin Elmer Pyris Diamond	238
Figure A.16 Atomic Absorption Spectrophotometer (AAS)/Atomic Emission Spectrophotometer (AES), Perkin Elmer Analyst 100	239
Figure A.17 Oven (Lindberg 0-1200 °C)	239

LIST OF ABBREVIATIONS

Symbols	Meaning
β	H – bond angle
ν	Stretching vibration (Wavenumber, cm^{-1})
$\nu_{\text{OH}}(\text{HOD})$	OH stretching of HOD molecule
$\nu_{\text{OD}}(\text{HOD})$	OD stretching of HOD molecule
δ	Bending vibration
ρ	Libration modes of water molecule (hindered rotations)
$\Delta\nu$	Frequency shift, where $\Delta\nu$ of vapor = 0
Γ	Distribution of the irreducible representation for a particular correlation field splitting
b	Broad peak
-dx	The sample has partially D isotope in form of HOD
ΔH_{H}	Enthalpy of hydrogen bonding ($\text{kJmol}^{-1}\text{OH}$)
DI	De-ionized water
$R_{\text{O} \dots \text{O}}$	The distance between oxygen of water and oxygen of anion group (PO_4^{3-})
s	Strong peak
sh	Shoulder peak
sp	Sharp peak
w	Weak peak
vs	Very strong peak
vw	Very weak peak
Z'	Number of molecules in the crystallographic cell
Z	Number of molecules in the Bravais of primitives cell
	$Z' = Z / \text{repeat units in cell}$